# Evolution Reversed: The Ability To Bind Iron Restored to the N-Lobe of the Murine Inhibitor of Carbonic Anhydrase by Strategic Mutagenesis[†]

Anne B. Mason,*[,‡] Gregory L. Judson,[§] Maria Cristina Bravo,[‡] Andrew Edelstein,[§] Shaina L. Byrne,[‡] Nicholas G. James,[‡] Eric D. Roush,[||,⊥] Carol A. Fierke,[#] Cedric E. Bobst,[+] Igor A. Kaltashov,[+] and Margaret A. Daughtery[§]

*Department of Biochemistry, College of Medicine, University of Vermont, Burlington, Vermont 05405, Program in Molecular Biology and Biochemistry, Middlebury College, Middlebury, Vermont 05753, Biochemistry Department, Duke University Medical School, Durham, North Carolina 27710, Chemistry Department and Biological Chemistry Department, University of Michigan, Ann Arbor, Michigan 48109, and Department of Chemistry, University of Massachusetts, Amherst, Massachusetts 01003*

*Received June 17, 2008; Revised Manuscript Received July 15, 2008*

ABSTRACT: The murine inhibitor of carbonic anhydrase (mICA) is a member of the superfamily related to the bilobal iron transport protein transferrin (TF), which binds a ferric ion within a cleft in each lobe. Although the gene encoding ICA in humans is classified as a pseudogene, an apparently functional ICA gene has been annotated in mice, rats, cows, pigs, and dogs. All ICAs lack one (or more) of the amino acid ligands in each lobe essential for high-affinity coordination of iron and the requisite synergistic anion, carbonate. The reason why ICA family members have lost the ability to bind iron is potentially related to acquiring a new function(s), one of which is inhibition of certain carbonic anhydrase (CA) isoforms. A recombinant mutant of the mICA (W124R/S188Y) was created with the goal of restoring the ligands required for both anion (Arg124) and iron (Tyr188) binding in the N-lobe. Absorption and fluorescence spectra definitively show that the mutant binds ferric iron in the N-lobe. Electrospray ionization mass spectrometry confirms the presence of both ferric iron and carbonate. At the putative endosomal pH of 5.6, iron is released by two slow processes indicative of high-affinity coordination. Induction of specific iron binding implies that (1) the structure of mICA resembles those of other TF family members and (2) the N-lobe can adopt a conformation in which the cleft closes when iron binds. Because the conformational change in the N-lobe indicated by metal binding does not impact the inhibitory activity of mICA, inhibition of CA was tentatively assigned to the C-lobe. Proof of this assignment is provided by limited trypsin proteolysis of porcine ICA.

The transferrins (TF)[1] are 80 kDa glycoproteins whose primary family members function in the transport of iron to cells and/or as bacteriostatic agents in a variety of biological fluids (*1*). Members of the TF family include serum transferrin (sTF), ovotransferrin (oTF) found in egg white, and lactoferrin (LTF) found in milk and other bodily secretions. The TF molecule is proposed to have evolved by gene duplication and fusion events resulting in two homologous lobes (*2*). Each lobe reversibly binds a single ferric ion coordinated to the side chains of two tyrosine residues, one histidine residue, one aspartate residue, and two oxygen atoms from a synergistic anion (carbonate) that is anchored by an arginine residue (*3*−*5*). Although the iron in each lobe of these family members is bound to identical ligands, the binding affinities differ considerably (10−100-fold) both between the family members and between lobes of any given family member (*6*−*8*) due to variations in the second shell residues (*9*).

Homology searches of DNA sequences have led to the discovery of additional members of the TF superfamily (*10, 11*). Some of these proteins do not appear to play a direct role in iron metabolism. For example, in bullfrogs, saxiphilin transports a neurotoxin called saxitoxin (*12*).

[†] This work is supported by U.S. Public Health Service Grants R01 DK 21739 (A.B.M.), GM 40602 (C.A.F.), and R01 GM061666 (I.A.K.). M.C.B. is supported by a National Institute of General Medical Sciences predoctoral fellowship (5F31GM081904). Support for S.L.B. and N.G.J. came from Hemostasis and Thrombosis Training Grant 5T32HL007594, issued to Dr. Kenneth G. Mann at the University of Vermont by the National Heart, Lung and Blood Institute.

* To whom correspondence should be addressed: Department of Biochemistry, University of Vermont, 89 Beaumont Ave., Burlington, VT 05405−0068. Telephone: (802) 656-0343. Fax: (802) 656-8220. E-mail: anne.mason@uvm.edu.

[‡] University of Vermont.

[§] Middlebury College.

[||] Duke University Medical School.

[⊥] Current address: BIAcore, Inc., Piscataway, NJ 08854.

[#] University of Michigan.

[+] University of Massachusetts.

[1] Abbreviations: TF, transferrin; sTF, serum transferrin; oTF, ovotransferrin; LTF, lactoferrin; mTF, melanotransferrin; hTF, human serum transferrin; $Fe_N$ hTF, N-His Y426F/Y517F hTF-NonGly, a His-tagged, nonglycosylated monoferric transferrin with iron only in the N-lobe (due to mutation of the Tyr residues in the C-lobe essential to iron binding); $Fe_C$ hTF, N-His Y95F/Y188F hTF-NonGly, a His-tagged nonglycosylated monoferric transferrin with iron only in the C-lobe; CA, carbonic anhydrase; CAII, carbonic anhydrase isoform II; mICA Gly, His-tagged glycosylated murine inhibitor of carbonic anhydrase; mICA NonGly, His-tagged nonglycosylated murine inhibitor of carbonic anhydrase; pICA, porcine inhibitor of carbonic anhydrase; BHK, baby hamster kidney; DMEM-F12, Dulbecco's modified Eagle's medium-Ham F-12; FBS, fetal bovine serum; UG, Ultroser G, a serum substitute; NTA, nitrilotriacetic acid; PNPA, *p*-nitrophenyl acetate; PNP, *p*-nitrophenyl; ESI-MS, electrospray ionization mass spectrometry; WT, wild-type.

10.1021/bi801133d CCC: $40.75 
Published on Web 08/20/2008

Table 1: Mutagenic Primers Used To Introduce the Mutations into mICA (mutated codons in bold)

| | |
|---|---|
| W124R forward | 5′-CTGGCCTGGG**CCG**GTCTGCTGGGTGG-3′ |
| S188Y forward | 5′-CCGGGAACCATACTTTGGC**TAC**TGGAGCC-3′ |
| T296K forward | 5′-GGGAGGACCTGCTGTTT**AAA**GATGCTGCTCATGGGC-3′ |
| N470D forward | 5′-CGTCCCCATGGGTTTAATATAC**GAT**CAAACTGGGTCTTGCAAATTTG-3′ |
| N645D forward | 5′-CACAGAATGTTTATCTAACCTTCAG**GAT**AAAACAACATATAAAACATACCTAGGACC-3′ |

However, for two other family members, melanotransferrin (mTF) (*13*) and the inhibitor of carbonic anhydrase (ICA) (*14*), the functions have been difficult to establish unambiguously.

As its name implies, ICA inhibits some isoforms of the enzyme carbonic anhydrase (CA). This enzyme catalyzes the reversible hydration of carbon dioxide to produce bicarbonate and a proton. Highly conserved CA is ubiquitous in living systems, playing roles in $CO_2$ transport, secretory processes, and calcification. The numerous mammalian isozymes of CA vary in activity, tissue localization, and physiological role (*15, 16*). CA inhibitory activity (indicative of the presence of ICA) has been detected in the serum from mice, rats, rabbits, cats, dogs, sheep, and pigs (*14, 17, 18*), but no inhibitory activity has yet been observed in human serum. To date, genes encoding ICA proteins have been found in pigs, mice, rats, cows, and dogs but not in marsupials, monotremes, avians, or fish. A gene corresponding to ICA in the human genome contains a premature stop codon and has therefore been annotated as a pseudogene (*19*). In many mammals, ICA is secreted into serum by hepatocytes to a concentration of ~1 $\mu$M. Due to mutations in one or more of the liganding residues in each lobe, neither porcine ICA (pICA) nor murine ICA (mICA) binds iron with high affinity (*14, 19*). Specifically, in the N-terminal lobe of mICA, the Tyr188 metal ligand is changed to Ser and the Arg124, which anchors the carbonate ligand, is changed to Trp. There is no direct evidence that the structure of ICA is the same as those of other TF family members, although the sequence of mICA is 59% identical (and 73% similar) to that of hTF, implying that the structures will be analogous. Phylogenetic analysis reveals that ICA is the most recently evolved member of the TF superfamily that appeared ~90 million years ago by tandem duplication of the TF gene (*10, 11*).

Here we use mutagenesis and biochemical studies to investigate the structural similarities between mICA and hTF and to determine which regions of mICA are important for inhibition of CA. We demonstrate that in mICA changing Trp124 to arginine and Ser188 to tyrosine, thereby recapitulating the metal site in hTF, recreates a high-affinity iron binding site. This result demonstrates that the structure of the N-terminal lobe of mICA is similar to that of hTF. However, the iron release parameters for this iron-binding mICA mutant differ compared to those of the N-terminal lobe of the hTF control, likely due to changes in the second shell residues in the N-lobe (*20*). The CA inhibitory activity of mICA is unchanged by iron binding to the N-terminal lobe of the double mutant, which should alter the structure of this region, or by removal of the carbohydrate moieties in the C-lobe. These data suggest that the C-terminal lobe of mICA interacts with human carbonic anhydrase isoform II (CAII). Consistent with this proposal, we demonstrate that a proteolytic fragment of pICA (72% identical to mICA) containing the C-lobe is sufficient for high-affinity binding of CAII.

## MATERIALS AND METHODS

*Materials.* The QuikChange mutagenesis kit was from Stratagene. Novablue (DE3) competent cells, Dulbecco's modified Eagle's medium-Ham F-12 nutrient mixture (DMEM-F12), antibiotic-antimycotic solution (100×), and a trypsin solution for cell release were from the GIBCO-BRL Life Technologies Division of Invitrogen. Either the Wizard MIDI prep kit from Promega or the Qiagen Mini prep kit was used for plasmid purification. Methotrexate from Bedford laboratories was purchased at a hospital pharmacy and used for selection of plasmid-containing cells. Fetal bovine serum (FBS) was obtained from Atlanta Biologicals. Ultroser G (UG) is a serum replacement from Pall BioSepra (Cergy, France). An Ultrasette tangential flow device with a 30 kDa molecular mass cutoff was from Pall Life Sciences. EDTA was from Mann Research Laboratories Inc. Ferrous ammonium sulfate and *p*-nitrophenyl acetate (PNPA) were from Sigma-Aldrich. Centricon 30 microconcentrators and Ultra-4 devices were from Millipore/Amicon. Ni-NTA Superflow resin was from Qiagen. A Sephacryl S-200HR column was obtained from Amersham Pharmacia. Trypsin was obtained from Boehringer Mannheim.

*Preparation of mICA Mutants.* The pNUT vector containing the cDNA for full-length mICA served as the mutagenesis template (*19*). As previously described, it contains the signal peptide from hTF, four amino acids from the amino terminus of hTF, a hexahistidine tag, and a Factor Xa cleavage site (*19*). A single mICA mutant with the S188Y mutation was first produced. A double mutant of mICA was made by introducing the W124R mutation into the plasmid already containing the S188Y mutant. A triple mutant was created by introducing the T296K mutation into the plasmid containing the W124R and S188Y mutations. Additionally, nonglycosylated forms of both the control mICA and the W124R/S188Y mICA mutant were made by substituting aspartic acid residues for the two asparagine residues (N470 and N645) predicted to serve as glycosylation sites. The mutagenic primers used to produce the various mutants are listed in Table 1.

In each case, the complete nucleotide sequence of the plasmid was verified prior to transfection of BHK cells (40−50% confluent) in 100 mm tissue culture dishes using the calcium phosphate method (*21*). During transfection and selection, cells were cultured in DMEM-F12 supplemented with 10% FBS. To begin selection, 0.44 mM methotrexate was added to the medium within 24 h of the transfection (all surviving cells were taken because we have determined that subcloning does not lead to greater protein production). Following the selection process, which usually takes 6−14 days, the transfected cells containing the pNUT plasmid were

expanded into flasks for transfer into roller bottles. Passage and expansion of cells have been previously described in detail (*22*).

*Production and Purification of Protein.* Production of recombinant mICA followed our standard protocol (*22*). Briefly, once in expanded surface roller bottles (1700 $cm^2$), the culture medium (200 mL/roller bottle) bathing the adherent BHK cells was collected every 2−3 days. The first three batches contained DMEM-F12 with 1× antibiotic-antimycotic solution and 10% FBS. Subsequent batches contained the same medium with 1% UG and 1 mM butyric acid replacing the FBS. UG contains a small amount of hTF (∼2−4 mg/L) and other proprietary additives. For reasons that are not understood, the presence of UG stimulates recombinant protein production to levels that are considerably higher than levels found in the presence of FBS. In addition, since UG has a smaller amount of other proteins compared to FBS, recombinant protein purification is simplified. Similarly, addition of butyric acid stimulates production of recombinant protein (*22*).

As previously described in detail, $Fe^{3+}$-NTA and $NaN_3$ were added to the pooled batches of medium (*22*). The collected batches were stored at 4 °C prior to purification. The medium was centrifuged at 6000*g* for 15 min and/or filtered through a plug of cotton to remove cell debris. Using a tangential flow device with a 30 kDa molecular mass cutoff filter, the medium was concentrated and exchanged into 5 mM Tris-HCl buffer (pH 8.0) containing 0.02% $NaN_3$. An appropriate amount of 5× Qiagen start buffer was added to yield a 1× solution [final concentration of 50 mM Tris (pH 7.5) containing 300 mM NaCl, 20 mM imidazole, 10% glycerol, and 0.05% $NaN_3$]. Following filtration through a 0.2 $\mu$M Acrocap filter, medium containing the recombinant protein was pumped at a rate of 2 mL/min onto a Ni-NTA column (1 cm × 10 cm) containing ∼7 mL of resin (binding capacity of 5−10 mg/mL). The column was attached to a BioCad Sprint system (Applied Biosystems) allowing for continuous monitoring of the absorbance at 280 nm, the conductivity, and the pH. Following sample loading, the column was washed with start buffer until the baseline returned to the background level (<0.05 $A_{280}$ unit). The His-tagged mICA constructs were displaced with elution buffer (Qiagen start buffer containing 250 mM imidazole); 3 mL fractions were collected. The eluted sample was pooled, concentrated, and applied to a Hi-Prep 26/60 Sephacryl S-200HR column in 100 mM $NH_4HCO_3$ to eliminate the imidazole, glycerol, and other buffer components. Monoferric N-His-tagged hTF constructs that bind iron only in the N-lobe (N-His Y426F/Y517F hTF-NonGly, designated $Fe_N$ hTF) or in the C-lobe (N-His Y95F/Y188F hTF NonGly, designated $Fe_C$ hTF) were similarly produced and purified. $Fe_N$ hTF served as a control for the W124R/S188Y mutant mICA construct since it binds iron only in the N-lobe (*19*). The homogeneity of the samples was assessed by SDS−polyacrylamide gel electrophoresis on 10% gels under reducing conditions and was visualized with Coomassie blue dye.

Porcine ICA (pICA) was purified from pig plasma using a CAII affinity column, and recombinant human CAII was expressed and purified from *Escherichia coli* as previously described in detail (*23*).

*Spectral Analysis.* Visible spectra of wild-type mICA and the mICA mutants in 100 mM $NH_4HCO_3$ were collected (between 550 and 350 nm) on a Varian Cary 100 spectrophotometer. Additionally, steady-state tryptophan fluorescence spectra were obtained using a Quantamaster-6 spectrofluorometer (Photon Technology International, South Brunswick, NJ) equipped with a 75 W xenon arc lamp excitation source, excitation/emission monochromators, a WG-295 nm cut-on excitation filter, and a WG-320 nm cut-on emission filter. Samples were excited at 295 nm, and emission scans were collected from 305 to 400 nm, using slit widths of 1 nm (excitation) and 4 nm (emission). Iron-containing protein (1 $\mu$M) was added to a cuvette (1.8 mL final volume) containing 100 mM HEPES buffer (pH 7.4) at 25 °C and gently stirred with a small magnetic stir bar. We obtained apoprotein by adding the same amount of iron protein to 100 mM MES (pH 5.6) containing 4 mM EDTA and 300 mM KCl and equilibrating until no further change in the spectrum was observed (*24*). Accurate molar absorption coefficients ($\varepsilon$) for apo- and iron-containing samples were determined as described in a recent protocol (*24, 25*).

*Analysis by Mass Spectrometry.* Samples of the recombinant mICA NonGly, the W124R/S188Y mICA NonGly mutant, and the human CAII−mICA NonGly complex were evaluated by ESI-MS under both near-native and denaturing conditions on a hybrid quadrupole/time-of-flight mass spectrometer (QStar-XL, MDS Sciex/Applied Biosystems, Toronto, ON) equipped with a standard Turbospray source. A 10 $\mu$M protein solution in 50 mM $NH_4HCO_3$ was continuously injected into the source at a flow rate of 3 $\mu$L/min. To observe the carbonate-bound complexes, the declustering potential was lowered. Typically, 150−300 scans were averaged for each spectrum to ensure an adequate signal-to-noise ratio. Protein denaturation was carried out using 50% MeOH and 5% glacial acetic acid.

*Kinetics of $Fe^{3+}$ Release.* The kinetics of iron release were monitored at pH 5.6 and 25 °C using an Applied Photophysics SX.18MV stopped-flow spectrofluorometer fitted with a 20 $\mu$L observation cell with a 2 nm light path and a dead time of ∼1.1 ms (*24*). One syringe contained protein (375 nM) in 300 mM KCl, and the other syringe contained 200 mM MES buffer (pH 5.6) with 300 mM KCl and 8 mM EDTA. The samples were excited at 280 nm (wavelength selection from a monochromator with a 9.3 nm band-pass), and fluorescence emission was monitored using a high-pass 320 nm cut-on filter. Rate constants were determined by fitting the change in fluorescence intensity versus time using Origin software (version 7.5).

*Assay for Carbonic Anhydrase Activity.* To evaluate the ability of the mICA and mICA mutants to inhibit human CAII, we adapted the colorimetric assay from the Sigma Aldrich website to a 1 mL format (http://www.sigmaaldrich.com/img/assets/18220/CarbonicAnhydrase-CSRD.pdf).

Our standard conditions included final concentrations of 9 mM Tris sulfate (pH 7.6), 1 mM PNPA, and 70 units of human CAII activity (1.5 $\mu$M). Following addition of the CAII (or the CAII preincubated with a stoichiometric amount of mICA), the increase in absorbance at 348 nm at 25 °C was monitored for 5 min on a Cary 100 spectrophotometer in double-beam mode using the temperature control feature. A cuvette containing only buffer and substrate served as the reference.

*Proteolysis of pICA by Trypsin.* Porcine ICA (0.23 mg/mL) was incubated with trypsin (0.02 mg/mL) in 50 mM

Table 2: Summary of Spectral Characteristics and Absorption Coefficients ($\varepsilon_{280}$, $mM^{-1}$ $cm^{-1}$) for the mICA Control and Double Mutant Compared to the Monoferric hTFs

| protein | $\lambda_{Max}$ (nm) | $A_{280}/A_{max}$ | calc[a] $\varepsilon_{280}$ (mM), apo | exp[b] $\varepsilon_{280}$ (mM), apo | exp[b] $\varepsilon_{280}$ (mM), iron | % increase due to iron[c] | % difference, apo calc/apo exp[d] |
|---|---|---|---|---|---|---|---|
| $Fe_N$ hTF | 471 | 44.4 | 82.1 | $81.4 \pm 0.3$ | $92.5 \pm 0.3$[e] | 13.6 | −0.9 |
| mICA glycosylated | none | − | 84.3 | $86.5 \pm 0.6$ | − | − | 1.2 |
| mICA Gly W124R/S188Y | 459 | 61.3 | 80.3 | $83.0 \pm 0.5$ | $91.9 \pm 0.8$ | 10.6 | 3.3 |
| mICA NonGly W124R/S188Y (N470D/N645D) | 457 | 71.9 | 80.3 | $80.5 \pm 0.2$ | $87.5 \pm 0.5$ | 9.1 | 0.2 |
| mICA Gly S188Y | none | − | 85.8 | $88.4 \pm 1.0$ | − | − | 2.9 |
| $Fe_C$ hTF | 461 | 42.2 | 82.1 | $81.5 \pm 0.2$ | $92.1 \pm 0.2$[e] | 13.0 | −0.7 |

[a] The absorption coefficients were calculated as described previously (*49*). [b] Determined as described by Edelhoch (*25, 50*). [c] Percent increase calculated as $100[\varepsilon(\text{iron}) - \varepsilon(\text{apo})]/\varepsilon(\text{apo})$. [d] Percent difference calculated as $100[\varepsilon(\text{apo}) - \varepsilon(\text{calc})]/\varepsilon(\text{apo})$. [e] From ref *25*.

$NaHCO_3$ (pH 8.0) containing 4 mM $CaCl_2$ for 75 min at 25 °C. The reaction was stopped by the addition of 0.4 mM phenylmethanesulfonyl fluoride. The completeness of the digestion was evaluated by SDS−PAGE using either a discontinuous buffer system or an 8 to 20% gradient gel with a continuous buffer system (Bio-Rad). Proteolytic fragments able to bind to CAII were isolated by incubation with CAII-Sepharose affinity resin (*23*). After application of the pICA fragments, the column was washed sequentially with 10 mM MOPS (pH 7.0), followed by 0.05 M NaSCN, 0.5 M NaSCN, and 1 M NaSCN all in 10 mM Tris-$SO_4$ (pH 8.0). Thiocyanate had previously been shown to elute pICA from this column (*23*). The eluate from the final step containing the most tightly bound peptides was concentrated and the NaSCN removed by ultrafiltration in a stirred cell (Amicon YM-10 molecular mass cutoff membrane). The peptides from this step were further fractionated by electrophoresis on a 15% SDS−PAGE gel with 11.4 mg/L sodium thioglycolate in the running buffer. Following transfer onto a polyvinyl difluoride membrane and staining with 2% Ponceau S, the membrane containing a 30 kDa fragment was excised, washed with water, and dried. The sequence of the peptide on this membrane was determined at the Harvard Microchemistry Facility.

## RESULTS AND DISCUSSION

Previous studies indicated that iron does not bind to either lobe of murine or porcine ICA (as predicted from the absence of conserved residues critical to iron and anion binding) (*14, 19*). The N-lobe of mICA has a tryptophan residue at position 124 and a serine residue at position 188. In the N-lobe of hTF, Arg124 stabilizes the synergistic carbonate anion and Tyr188 is a ligand to the iron (*26*). Previous mutational analysis of the N-lobe of hTF demonstrated that mutation of Arg124 to alanine weakens iron binding (but does not preclude it), whereas mutation of Tyr188 to phenylalanine completely eliminates iron binding (*27*). Protonation of the bound carbonate ligand is the initiating step of iron release (*28*), and the position of the flexible Arg124 relative to the carbonate has a considerable effect on the rate constant for iron release (*26*). Given this information, a single mutant of mICA, S188Y, was made to restore the critical tyrosine ligand and allow determination of whether a Trp residue at position 124 is compatible with iron binding in this context. Additionally a W124R/S188Y double mutant of mICA was produced to assess whether the N-lobe of this family member could be induced to bind iron if both of the residues found in the hTF N-lobe were restored. We hypothesized that the three-dimensional structure of mICA might be similar enough to hTF to allow the capture of iron when the liganding residues were reintroduced.

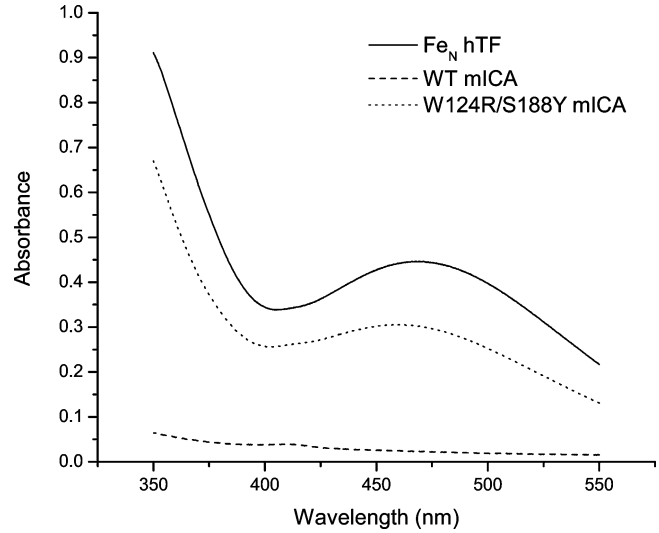


FIGURE 1: UV−vis spectra of $Fe_N$ hTF, mICA, and iron-containing W124R/S188Y wild-type (WT) mICA. Purified proteins (~200 $\mu$M) in 100 mM $NH_4HCO_3$ were scanned between 550 and 350 nm.

*Absorbance Spectra.* Initial characterization of iron binding is provided by the UV−visible spectra of the hTF or mICA control and the various mICA mutants. A visible absorption band at ~470 nm is produced when iron binds to TF family members. This ligand to metal charge transfer band results from the interaction of ferric iron with the oxygens of the two tyrosine ligands. The spectral parameters and calculated and experimental molar absorption coefficients are presented in Table 2. The absence of a visible absorbance signal for both the wild-type and the S188Y mICA (data not shown) mutant clearly shows that iron does not bind to these proteins. However, the glycosylated mICA containing the W124R/S188Y double mutant has a visible absorbance maximum at 459 nm which is hypsochromically shifted to 457 nm in the nonglycosylated form of this mutant (Figure 1 and Table 2), demonstrating that this mutant does bind $Fe^{3+}$. The spectral parameters of the W124R/S188Y double mutant did not change upon addition of several aliquots of $Fe^{3+}$-NTA, indicating that the metal site is saturated. Interestingly, the visible maximum is more similar to that found for hTF with iron bound to only the C-lobe (461 nm) than to that found for hTF with iron bound to only the N-lobe (471 nm) (*22*). Differences in the absorbance maxima can be attributed to subtle alterations in the geometry of the metal ligands (particularly the relationship of the iron to the two tyrosine ligands) (*29*). Additionally, as described in the discussion of the fluorescence spectra below, the differences in the

number and position of the tryptophan residues affect the absorbance maxima.

The spectral data demonstrate that two amino acid substitutions in the metal site, W124 and S188, are responsible for the lack of iron binding to wild-type mICA and that the overall structure of mICA is sufficiently similar to hTF to allow high-affinity iron binding upon restoration of the metal site ligands. In the structure of the isolated apo N-lobe of hTF (*30*), the two Tyr ligands are 3.9 Å apart with their OH groups projecting into the binding cleft in the proximity of Arg124 (and the terminus of α-helix 5) such that these residues are well positioned to capture iron and the synergistic carbonate. Once the $Fe^{3+}$ and carbonate bind, movement of Arg124 is required to lock in the carbonate (and eliminate the chelator, NTA). The side chains of Asp63 and His249 fill out the octahedral coordination of the bound $Fe^{3+}$. The spectral data for the iron-bound W124R/S188Y double mutant strongly support the assumption that a similar iron coordination sphere occurs in this protein: Tyr95, Tyr188, His249, Asp63, and two oxygens from bicarbonate. In particular, the visible maximum (Table 2) is consistent with a full complement of ligands since single mutants of the N-lobe of hTF lacking Asp63, Tyr95, or His249 have visible maxima that are hypsochromically shifted ($A_{max}$ ~ 420 nm), and these mutants are yellow in color (*20*). In the absence of a crystal structure, an alternative possibility to the spectral properties of the mICA double mutant is that the chelator NTA (which keeps the $Fe^{3+}$ in solution) is not displaced from the iron and might provide ligands to it (as observed in a structure of the N-lobe of oTF) (*31*). In this structure, the Asp and His ligands and the synergistic anion do not participate in the coordination sphere. However, the spectral properties (Table 2), the ESI results, and the kinetics of release of iron (see below) from the mICA double mutant indicate that NTA is, in fact, displaced and suggest that the Asp63 and His249 liganding residues, which are conserved in mICA, participate in the coordination of the iron.

*Mass Spectrometry Analyses.* ESI-MS analysis of the nonglycosylated mICA samples was carried out under both denaturing and near-native conditions (Figure 2). The charge-state distribution of protein ions under denaturing conditions is very broad, which is typical of unfolded proteins (*32*). ESI-MS experiments carried out under denaturing conditions routinely provide information about the polypeptide mass with an accuracy of ≤0.01%, and as shown in Table 3, there is excellent agreement between the measured mass of the double mutant mICA and the mass calculated from the protein sequence. The protein ion charge-state distribution under native conditions is narrow, and the average number of charges is low, consistent with the notion of a tightly folded protein. ESI-MS measurements carried out under such conditions allow both the composition and stoichiometry of metalloprotein complexes to be established (*33*). The spectrum shows unequivocally that $Fe^{3+}$ is bound to the W124R/S188Y mICA double mutant (Figure 2). Additionally, a small amount of the ternary complex (with the labile carbonate) can also be observed under mild ion desolvation conditions at the ESI interface. The relatively low abundance of ions representing the ternary complex is consistent with the facile dissociation of the synergistic anions from the N-lobe of hTF previously reported (*34*). Analysis of the human CAII−mICA NonGly complex indicates the presence of both species at a

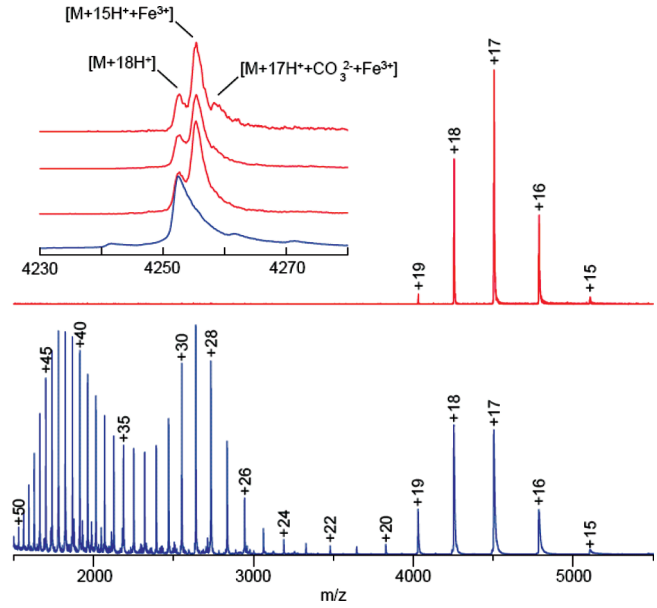


FIGURE 2: ESI mass spectra of mICA NonGly double mutant W124R/S188Y. Spectra were collected under near-native (red trace) or denaturing (blue trace) conditions. Representative ions have been labeled by charge state. The inset expands the region around the +18 charged ions and highlights the appearance of carbonate as the conditions become increasingly milder (from bottom to top).

Table 3: Determination of Masses by Electrospray Mass Spectrometry

| protein | solution | measured mass (Da) | calculated average mass[a] (Da) |
|---|---|---|---|
| mICA NonGly[a] | denaturing | 76487 ± 9.3 | 76482 |
| mICA NonGly W124R/S188Y, iron-saturated | denaturing | 76527 ± 7.4 | 76527 |
| mICA NonGly W124R/S188Y, iron-saturated | near-native ($Fe^{3+}$ present) | 76583 ± 10.8 | 76583 |
| mICA NonGly with human CAII | near-native | 105714 ± 13.2 | 105728 |

[a] The calculated mass of mICA (residues 1−681) nonglycosylated (N470D, N645D) is 74795 Da, to which is added 440 Da for the V-P-D-K sequence, 823 Da for the hexa-His tag, and 456 Da for the Factor Xa cleavage sequence (IEGR), for a total mass of 76514 Da. Because the 32 Cys residues are all engaged in disulfide bonds, 32 H atoms are subtracted to yield the calculated mass. Human CAII has a calculated mass of 29246 Da.

1:1 stoichiometry (Table 3), as reported previously for the bovine CAII−mICA Gly complex (*19*)

*Fluorescence Spectra.* Further characterization is provided by steady-state fluorescence spectra of the proteins in the presence or absence of iron (Figure 3). It is well-established that coordination of iron quenches the intrinsic fluorescence attributed to tryptophan residues in hTF. The N-lobe of hTF has three tryptophan residues (at positions 8, 128, and 264). We have recently shown that only Trp128 and Trp264 make significant contributions to the fluorescence spectrum of the isolated hTF N-lobe (*24*). Thus, in the case of the N-lobe of hTF, iron release is reported by the increase in the intrinsic fluorescence of both Trp128 and Trp264. Significantly, the N-lobe of mICA has four tryptophan residues (at positions 8, 124, 128, and 189). In contrast, the C-lobes of hTF and mICA both have a total of five tryptophan residues at equivalent positions. Thus, compared to hTF, the only difference is the number and distribution of the Trp residues

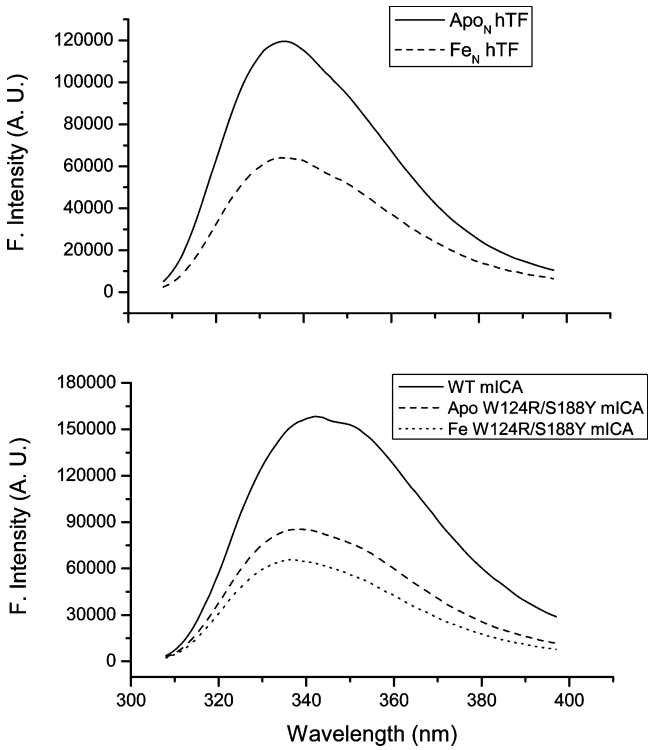


FIGURE 3: Steady-state fluorescence emission spectra of Fe$_N$ hTF, mICA, and the mICA double mutant. Iron-containing samples (1 $\mu$M) were scanned (305−400 nm) in 100 mM HEPES (pH 7.4) (excitation at 295 nm and emission with a 320 nm cut-on filter). Scans of iron free samples were obtained following addition of an equal concentration of each protein to 100 mM MES (pH 5.6) containing 4 mM EDTA and 300 mM KCl and incubation for 20 min to ensure complete iron removal.

in the N-lobe of mICA. As shown in Figure 3, the fluorescence spectrum of the mICA control has a greater intensity and a red-shifted $\lambda_{max}$ (343 nm) relative to that of apo-hTF (335 nm). In mICA, the proximity of Trp124 to Trp128, the presence of a tryptophan residue at a new position (Trp189) adjacent to the missing Tyr188 ligand, and the absence of Trp264 all clearly have a cumulative effect on the fluorescence properties in comparison to those of hTF. In the double mICA mutant, Trp124 has been eliminated by mutation to arginine. Examination of the apo double mutant reveals a considerable reduction in the fluorescence intensity compared to the mICA control (a 35% decrease) and a 4 nm blue shift in the maximum. As with the absorbance spectra, it is clear that there are substantial differences between Fe$_N$ hTF and the iron binding double mICA mutant, the most striking of which is the percent increase in the fluorescence intensity in transitioning from the iron to the apo form. The mICA double mutant experiences only a 30% increase in fluorescence compared to a 76% increase for Fe$_N$ hTF. The absence of Trp264 from mICA provides a reasonable explanation for the reduction in the magnitude of the fluorescence signal when iron is released from the mICA double mutant.

*Kinetics of Iron Release.* Iron release was assessed at the putative endosomal pH of 5.6 under our "standard" conditions. Typical iron release curves for Fe$_N$ hTF and the double mICA mutant (with and without carbohydrate) are presented in Figure 4. For Fe$_N$ hTF, a triple-exponential function provides an excellent fit of the data, yielding rate constants presented in Table 4. For the double mICA Gly mutant, a

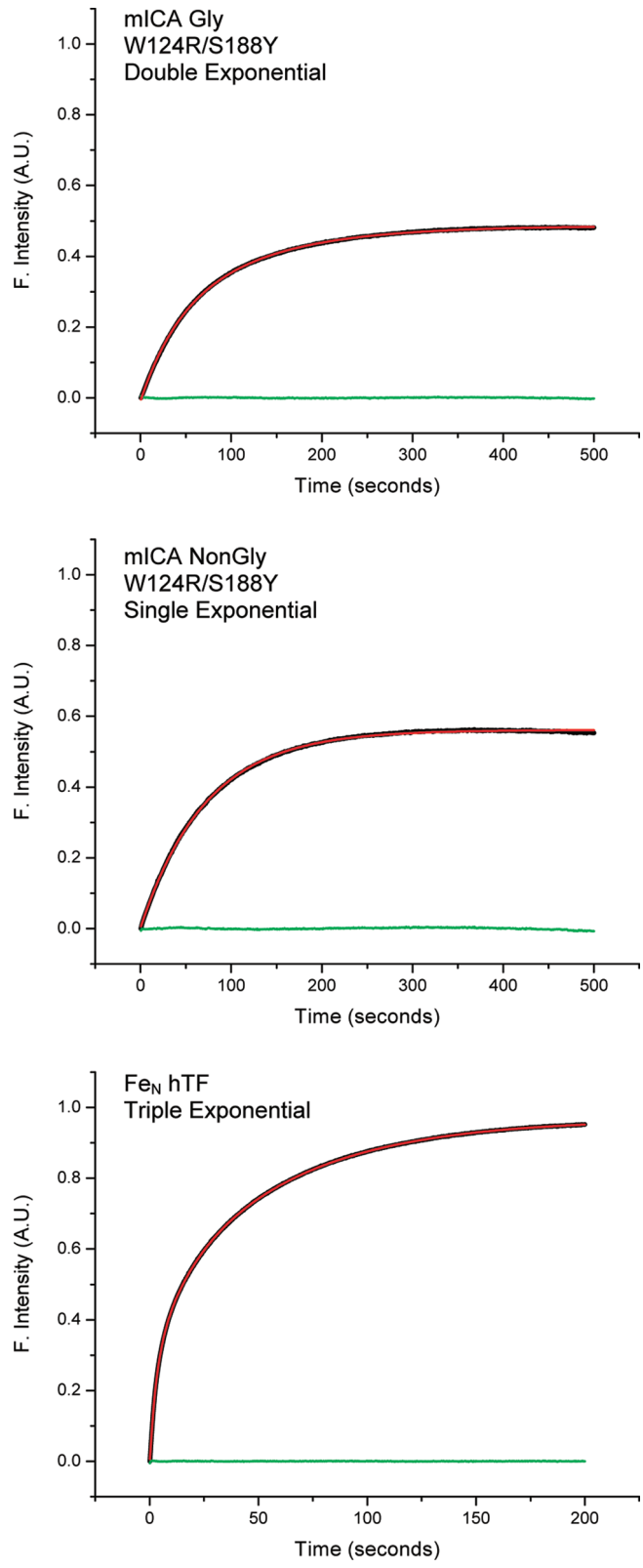


FIGURE 4: Kinetics of release of iron from Fe$_N$ hTF, the Fe W124R/S188Y mICA Gly mutant, and the Fe W124R/S188Y mICA NonGly mutant. Each curve is an average of at least five runs. Samples (375 nM in 300 mM KCl) were mixed in a stopped-flow spectrofluorometer with 200 mM MES (pH 5.6), 8 mM EDTA, and 300 mM KCl. Excitation was at 280 nm, and tryptophan emission was monitored by use of a 320 nm cut-on filter. The black curves show the original trace. The red curves indicate the fits, and the green line shows the residuals for the various fits. Note the different time scales.

Table 4: Summary of Kinetic Data for the mICA Double Mutant with and without Glycosylation Compared $Fe_N$ hTF under Standard Conditions [100 mM MES (pH 5.6) with 4 mM EDTA and 300 mM KCl]

| protein | $k_{obsN1}$ ($min^{-1}$) | $k_{obsN2}$ ($min^{-1}$) | $k_{obsN3}$ ($min^{-1}$) | $I_1$, $I_2$, $I_3$ (%)[a] | $n$[b] |
|---|---|---|---|---|---|
| mICA Gly W124R/S188Y | 1.64 ± 0.38 | 0.49 ± 0.11 | − | 39/61 | 9 |
| mICA NonGly W124R/S188Y | 0.83 ± 0.02 | − | − | 100 | 6 |
| $Fe_N$ hTF | 20.8 ± 5.6 | 4.11 ± 1.04 | 1.05 ± 0.09 | 25/22/53 | 35 |

[a] $I_1$, $I_2$, and $I_3$ refer to the change in intensity corresponding to $k_{obsN1}$, $k_{obsN2}$, and $k_{obsN3}$. [b] Number of replicates.

double-exponential function provides the best fit and yields two relatively slow rate constants. Interestingly, the NonGly mICA double mutant fits best to a single-exponential function with a rate constant that falls between the two rate constants found for the glycosylated double mutant. The rate constants for release of iron from the mICA mutants are thus similar to the slowest rate constant that accounts for approximately half of the intensity change in the $Fe_N$ hTF control. The fact that carbohydrate in the C-lobe appears to have some effect on the release of iron from the N-lobe is consistent with evidence that the two lobes of many different TF family members communicate with each other in a cooperative manner (either positive or negative) (*35*−*38*). (A complete analysis of the complex kinetics found for $Fe_N$ hTF and $Fe_C$ hTF will be the subject of another report.)

The crucial finding from the kinetic experiments is that the iron release parameters for the double mICA mutants differ compared to those of the $Fe_N$ hTF control, indicating a difference in the pathway leading to iron release. Certainly the absence of Trp264 in mICA as a reporter of iron release is one possibility. Another obvious difference is the presence of a threonine residue at position 296 in the mICA mutant instead of the lysine found in hTF. Thr296 is the first residue in the completely conserved TXA motif found in all six ICA sequences (ref *19*, supplement) in place of the KXS motif present in most other TF family members. Lys296 comprises half of the dilysine trigger critical to the mechanism of release of iron from the N-lobe of hTF. In the N-lobes of both hTF and oTF, this lysine comes together with another lysine (206, human numbering) in the iron-bound protein at neutral pH and shares a hydrogen bond. When the proteins encounter the lower pH in the endosome, the influx of hydrogen ions causes these two lysines to repel each other, thereby triggering the opening of the cleft (*39, 40*).

We attempted to test the idea that the absence of the dilysine trigger accounts for some of the difference in iron release by producing a triple mICA mutant (W124R/S188Y/T296K) with the lysine residue at position 296 added. Unfortunately (and quite unexpectedly), protein production of the triple mutant was too low to isolate enough pure protein for spectral and kinetic evaluation. Although it is not possible to explain why the substitution of lysine for threonine at this position would have such a profound effect on mICA production, it is curious that this particular threonine is one of only three conserved residues in the N-lobe unique to ICA (see above). Previously, expression of numerous mutants of both hTF and the N-lobe has been robust except when multiple tryptophan residues were replaced with other residues (*24*). The inability of the recombinant mICA to tolerate the threonine to lysine change at position 296 again appears to highlight the subtle differences in the three-dimensional structure of family members.

*CAII Assay.* Using a standard colorimetric assay, we demonstrated that a stoichiometric amount of mICA (glycosylated or nonglycosylated) or the mICA double mutant is equally effective at inhibiting the activity of human CAII. For CAII alone, the specific activity for catalysis of hydrolysis of *p*-nitrophenylacetate is 72 ± 4 mol of PNP per second per mole of CAII. Upon addition of a stoichiometric concentration of various forms of mICA, the specific activity decreases nearly to background: 1.1 ± 0.1 for the CAII−mICA Gly complex, 1.1 ± 0.1 for the CAII−mICA NonGly complex, and 1.2 ± 0.1 for the CAII−mICA W124R/S188Y mutant complex with iron bound to the N-lobe. Retention of inhibition by mICA even with iron bound to the N-lobe, which should alter the structure of this region, suggests that the inhibitory activity may reside in the C-lobe of mICA and that the presence or absence of carbohydrate in the C-lobe has no effect on the inhibition.

*Limited Proteolysis of pICA Allows Assignment of the Inhibitory Activity to the C-Lobe.* Since ICA is twice the size of CAII, it is possible that only one of the two halves of ICA is required for inhibition. To definitively determine whether the inhibitory activity could be assigned to the C-lobe, the highly homologous protein, pICA, isolated from pig serum, was incubated with trypsin. Both the loss of the CAII inhibitory activity (assayed as described above) and proteolysis of pICA as a function of time were measured. Following incubation with trypsin for 75 min, ∼50% of the inhibitory activity of pICA remains while less than 20% of intact pICA can be observed by SDS−PAGE (data not shown). The product of the limited trypsin digest was combined with CAII-Sepharose to bind any proteolytic fragments that retain high affinity for CAII. After sequential washes of the column with buffers containing 0.05 M NaSCN and 0.5 M NaSCN, the fragments with the highest avidity were eluted with buffer containing 1 M NaSCN. SDS−PAGE revealed two fragments with molecular masses of ∼45 and 30 kDa. Nonreducing native gel electrophoresis showed that these two fragments are not linked by disulfide bonds, suggesting that the inhibitory activity of pICA resides in a peptide of pICA with a mass of ∼30 kDa. This fragment was fractionated by electrophoresis and electroblotted onto a PVDF membrane, and the N-terminal amino acid sequence was determined to be FGSKC VNTPV EGYYV VAVVK KSDAD. Translation of the nucleotide sequence of pICA (*14*) shows that this peptide corresponds to amino acids 417−441, thereby assigning the inhibitory activity to the C-lobe. We calculate that a peptide from residue 417 to the final amino acid at position 685 has a molecular mass of 29717 Da, showing reasonable correspondence with the mass estimated from the SDS−PAGE gel. The cleft of the C-lobe of hTF is comprised of two subdomains C1 (residues 339−425 and 573−679 in hTF and residues 338−428 and 580−685 in pICA) and C2 (residues 426−572 in hTF and residues 429−579 in pICA). Thus, the isolated CAII binding fragment comprises all of the C2 subdomain and much of the C1 subdomain.

As with saxiphilin, the N-lobe of ICA is retained even though it does not appear to be necessary for ligand binding. A possible physiological role for ICA might be to rescue

CAII from excretion by the kidney glomeruli for preferential delivery to the liver (and this role would require both lobes). This suggestion is consistent with evidence that intact hen oTF is retained by the kidneys but the isolated N- and C-terminal lobes (each ≈40 kDa) of hen oTF are secreted into the urine when oTF is injected into mice (*41*). A second suggestion is that the N-lobe might be required for interaction with (unidentified) hepatic receptors critical for transport of the CA−ICA complex from plasma to liver possibly to recover zinc from the breakdown of CAII. Additionally, the N-lobe of ICA might have a function unrelated to the CAII inhibitory activity of the protein. Other instances of TF family members with secondary activities not associated with their iron binding capacity exist. For example, it has been reported that LTF binds DNA with distinct sequence specificity (*42*) and that horse apo-TF specifically supports the growth of thyroid hormone-dependent pituitary tumor cell cultures in chemically defined serum free media, while horse diferric TF completely inhibits growth of these cultures (*43*).

*Evolution of ICA.* Understanding the significance of ICA as an evolutionarily recent addition to the TF superfamily is complex since it involves both the appearance of a duplicated gene which is maintained in some species (mouse, rat, dog, pig, and cow), has been lost from others (primates), and never appeared in still others (fish, birds, etc.). Both gene duplication and gene loss are recurring themes in evolution leading to diversity (*44*−*46*). Since the function(s) of ICA is not completely clear, it is difficult to speculate about how its loss might confer any advantage. In broad terms, loss of genes from the human genome is often associated with either the immune system or chemotaxis. For example, the "pseudogenization" of the gene encoding CASPASE12 confers an advantage by making humans less susceptible to sepsis (*46*). Because there is a growing body of evidence that the founding family members of the TF family are intimately involved with the immune system (*47, 48*), it is possible that the emergence of ICA may be related to innate immunity since the role of zinc in the immune system is well-established.

In summary, we have produced a double mutant of mICA (glycosylated and nonglycosylated) that can bind and release iron from the N-lobe. This finding indicates that the structure of mICA is similar to those of the other TF family members, thereby bringing the appropriate and required residues into proximity to bind and hold the ferric ion. As with other family members, this implies a dynamic equilibrium in which the cleft can sample open and closed conformations. The availability of iron (and the ligands needed for coordination) results in a closed cleft prescribed by the high affinity of the liganding residues and synergistic anion for ferric iron. The loss of the ability to bind iron in the ICA family members is presumably related to acquisition of a new function(s). In the N-lobe, the substitution of a conserved tryptophan residue at position 124 in all of the ICA sequences to date is particularly intriguing. Since the N-lobe does not appear to be required for inhibition of CAII, the significance of the conserved tryptophan residue at this key position is unexplained.

## ACKNOWLEDGMENT

We owe tremendous thanks to Drs. Fudi Wang and Nancy C. Andrews at Children's Hospital Boston and Harvard Medical School (Boston, MA) for initiating the work on mouse ICA and to Drs. Tanya Griffiths and Ross MacGillivray at the Department of Biochemistry and Molecular Biology and Centre for Blood Research, University of British Columbia (Vancouver, BC), for producing the plasmid to allow expression of mICA. We thank Dr. Lisa Lambert at Chatham University for her expertise in the evolution of the transferrin superfamily.

## REFERENCES

1. Aisen, P., Enns, C., and Wessling-Resnick, M. (2001) Chemistry and biology of eukaryotic iron metabolism. *Int. J. Biochem. Cell Biol. 33*, 940–959.
2. Park, I., Schaeffer, E., Sidoli, A., Baralle, F. E., Cohen, G. N., and Zakin, M. M. (1985) Organization of the human transferrin gene: Direct evidence that it originated by gene duplication. *Proc. Natl. Acad. Sci. U.S.A. 82*, 3149–3153.
3. Anderson, B. F., Baker, H. M., Dodson, E. J., Norris, G. E., Rumball, S. V., Waters, J. M., and Baker, E. N. (1987) Structure of human lactoferrin at 3.2 Å resolution. *Proc. Natl. Acad. Sci. U.S.A. 84*, 1769–1773.
4. Kurokawa, H., Mikami, B., and Hirose, M. (1995) Crystal structure of diferric hen ovotransferrin at 2.4 Å resolution. *J. Mol. Biol. 254*, 196–207.
5. Hall, D. R., Hadden, J. M., Leonard, G. A., Bailey, S., Neu, M., Winn, M., and Lindley, P. F. (2002) The crystal and molecular structures of diferric porcine and rabbit serum transferrins at resolutions of 2.15 and 2.60 Å, respectively. *Acta Crystallogr. D58*, 70–80.
6. Princiotto, J. V., and Zapolski, E. J. (1975) Difference between the two iron-binding sites of transferrin. *Nature 255*, 87–88.
7. Lestas, A. N. (1976) The effect of pH upon human transferrin: Selective labelling of the two iron-binding sites. *Br. J. Haematol. 32*, 341–350.
8. Halbrooks, P. J., He, Q. Y., Briggs, S. K., Everse, S. J., Smith, V. C., MacGillivray, R. T. A., and Mason, A. B. (2003) Investigation of the mechanism of iron release from the C-lobe of human serum transferrin: Mutational analysis of the role of a pH sensitive triad. *Biochemistry 42*, 3701–3707.
9. Baker, H. M., Anderson, B. F., Brodie, A. M., Shongwe, M. S., Smith, C. A., and Baker, E. N. (1996) Anion binding by transferrins: Importance of second-shell effects revealed by the crystal structure of oxalate-substituted diferric lactoferrin. *Biochemistry 35*, 9007–9013.
10. Lambert, L. A., Perri, H., and Meehan, T. J. (2005) Evolution of the duplications in the transferrin family of proteins. *Comp. Biochem. Physiol., Part B: Biochem. Mol. Biol. 140*, 11–25.
11. Lambert, L. A., Perri, H., Halbrooks, P. J., and Mason, A. B. (2005) Evolution of the transferrin family: Conservation of residues associated with iron and anion binding. *Comp. Biochem. Physiol., Part B: Biochem. Mol. Biol. 142*, 129–141.
12. Morabito, M. A., and Moczydlowski, E. (1994) Molecular cloning of bullfrog saxiphilin: A unique relative of the transferrin family that binds saxitoxin. *Proc. Natl. Acad. Sci. U.S.A. 91*, 2478–2482.
13. Rose, T. M., Plowman, G. D., Teplow, D. P., Dreyer, W. J., Hellstrom, K. E., and Brown, T. P. (1986) Primary structure of the human melanoma-associated antigen p97 (melanotransferrin) deduced from the mRNA sequence. *Proc. Natl. Acad. Sci. U.S.A. 83*, 1261–1265.
14. Wuebbens, M. W., Roush, E. D., Decastro, C. M., and Fierke, C. A. (1997) Cloning, sequencing, and recombinant expression of the porcine inhibitor of carbonic anhydrase: A novel member of the transferrin family. *Biochemistry 36*, 4327–4336.
15. Tashian, R. E. (1992) Genetics of the mammalian carbonic anhydrases. *Adv. Genet. 30*, 321–356.
16. Tripp, B. C., Smith, K., and Ferry, J. G. (2001) Carbonic anhydrase: New insights for an ancient enzyme. *J. Biol. Chem. 276*, 48615–48618.
17. Booth, V. H. (1938) The carbonic anhydrase inhibitor in serum. *J. Physiol. 91*, 474–489.
18. Hill, E. P. (1986) Inhibition of carbonic anhydrase by plasma of dogs and rabbits. *J. Appl. Physiol. 60*, 191–197.
19. Wang, F., Lothrop, A. P., James, N. G., Griffiths, T. A., Lambert, L. A., Leverence, R., Kaltashov, I. A., Andrews, N. C., MacGillivray, R. T., and Mason, A. B. (2007) A novel murine protein with no

effect on iron homeostasis is homologous to transferrin and is the putative inhibitor of carbonic anhydrase. *Biochem. J. 406*, 85–95.
20. He, Q. Y., Mason, A. B., and Templeton, D. M. (2002) Molecular aspects of release of iron from transferrins. In *Molecular and Cellular Iron Transport*, pp 95−123, Marcel Dekker, Inc., New York.
21. Mason, A. B., Funk, W. D., MacGillivray, R. T. A., and Woodworth, R. C. (1991) Efficient production and isolation of recombinant amino-terminal half-molecule of human serum transferrin from baby hamster kidney cells. *Protein Expression Purif. 2*, 214–220.
22. Mason, A. B., Halbrooks, P. J., Larouche, J. R., Briggs, S. K., Moffett, M. L., Ramsey, J. E., Connolly, S. A., Smith, V. C., and MacGillivray, R. T. A. (2004) Expression, purification, and characterization of authentic monoferric and apo-human serum transferrins. *Protein Expression Purif. 36*, 318–326.
23. Roush, E. D., and Fierke, C. A. (1992) Purification and characterization of a carbonic anhydrase II inhibitor from porcine plasma. *Biochemistry 31*, 12536–12542.
24. James, N. G., Berger, C. L., Byrne, S. L., Smith, V. C., MacGillivray, R. T. A., and Mason, A. B. (2007) Intrinsic fluorescence reports a global conformational change in the N-lobe of human serum transferrin following iron release. *Biochemistry 46*, 10603–10611.
25. James, N. G., and Mason, A. B. (2008) Protocol to determine accurate absorption coefficients for iron containing transferrins. *Anal. Biochem. 378*, 202–207.
26. Adams, T. E., Mason, A. B., He, Q. Y., Halbrooks, P. J., Briggs, S. K., Smith, V. C., MacGillivray, R. T., and Everse, S. J. (2003) The position of arginine 124 controls the rate of iron release from the N-lobe of human serum transferrin. A structural study. *J. Biol. Chem. 278*, 6027–6033.
27. He, Q. Y., Mason, A. B., Woodworth, R. C., Tam, B. M., MacGillivray, R. T. A., Grady, J. K., and Chasteen, N. D. (1997) Inequivalence of the two tyrosine ligands in the N-lobe of human serum transferrin. *Biochemistry 36*, 14853–14860.
28. MacGillivray, R. T. A., Moore, S. A., Chen, J., Anderson, B. F., Baker, H., Luo, Y. G., Bewley, M., Smith, C. A., Murphy, M. E., Wang, Y., Mason, A. B., Woodworth, R. C., Brayer, G. D., and Baker, E. N. (1998) Two high-resolution crystal structures of the recombinant N-lobe of human transferrin reveal a structural change implicated in iron release. *Biochemistry 37*, 7919–7928.
29. Patch, M. G., and Carrano, C. J. (1981) The origin of the visible absorption in metal transferrins. *Inorg. Chim. Acta 56*, L71–L73.
30. Jeffrey, P. D., Bewley, M. C., MacGillivray, R. T. A., Mason, A. B., Woodworth, R. C., and Baker, E. N. (1998) Ligand-induced conformational change in transferrins: Crystal structure of the open form of the N-terminal half-molecule of human transferrin. *Biochemistry 37*, 13978–13986.
31. Mizutani, K., Yamashita, H., Kurokawa, H., Mikami, B., and Hirose, M. (1999) Alternative structural state of transferrin: The crystallographic analysis of iron-loaded but domain-opened ovotransferrin N-lobe. *J. Biol. Chem. 274*, 10190–10194.
32. Kaltashov, I. A., and Abzalimov, R. R. (2008) Do ionic charges in ESI MS provide useful information on macromolecular structures? *J. Am. Soc. Mass Spectrom. 19*, 1238–1245.
33. Kaltashov, I. A., Zhang, M., Eyles, S. J., and Abzalimov, R. R. (2006) Investigation of structure, dynamics and function of metalloproteins with electrospray ionization mass spectrometry. *Anal. Bioanal. Chem. 386*, 472–481.
34. Gumerov, D. R., and Kaltashov, I. A. (2001) Dynamics of iron release from transferrin N-lobe studied by electrospray ionization mass spectrometry. *Anal. Chem. 73*, 2565–2570.
35. Bali, P. K., and Harris, W. R. (1989) Cooperativity and heterogeneity between the two binding sites of diferric transferrin during iron removal by pyrophosphate. *J. Am. Chem. Soc. 111*, 4457–4461.
36. Bali, P. K., and Aisen, P. (1992) Receptor-induced switch in site-site cooperativity during iron release by transferrin. *Biochemistry 31*, 3963–3967.
37. Gumerov, D. R., Mason, A. B., and Kaltashov, I. A. (2003) Interlobe communication in human serum transferrin: Metal binding and conformational dynamics investigated by electrospray ionization mass spectrometry. *Biochemistry 42*, 5421–5428.
38. Hamilton, D. H., Turcot, I., Stintzi, A., and Raymond, K. N. (2004) Large cooperativity in the removal of iron from transferrin at physiological temperature and chloride ion concentration. *J. Biol. Inorg. Chem. 9*, 936–944.
39. Dewan, J. C., Mikami, B., Hirose, M., and Sacchettini, J. C. (1993) Structural evidence for a pH-sensitive dilysine trigger in the hen ovotransferrin N-lobe: Implications for transferrin iron release. *Biochemistry 32*, 11963–11968.
40. He, Q. Y., Mason, A. B., Tam, B. M., MacGillivray, R. T. A., and Woodworth, R. C. (1999) Dual role of Lys206-Lys296 interaction in human transferrin N-lobe: Iron-release trigger and anion-binding site. *Biochemistry 38*, 9704–9711.
41. Williams, J., Grace, S. A., and Williams, J. M. (1982) Evolutionary significance of the renal excretion of transferrin half-molecule fragments. *Biochem. J. 201*, 417–419.
42. He, J., and Furmanski, P. (1995) Sequence specificity and transcriptional activation in the binding of lactoferrin to DNA. *Nature 373*, 721–724.
43. Sirbasku, D. A., Stewart, B. H., Pakala, R., Eby, J. E., Sato, H., and Roscoe, J. M. (1991) Purification of an equine apotransferrin variant (thyromedin) essential for thyroid hormone dependent growth of GH 1 rat pituitary tumor cells in chemically defined culture. *Biochemistry 30*, 295–304.
44. Davis, J. C., and Petrov, D. A. (2004) Preferential duplication of conserved proteins in eukaryotic genomes. *PLoS Biol. 2*, E55.
45. Olson, M. V. (1999) When less is more: Gene loss as an engine of evolutionary change. *Am. J. Hum. Genet. 64*, 18–23.
46. Wang, X., Grus, W. E., and Zhang, J. (2006) Gene losses during human origins. *PLoS Biol. 4*, e52.
47. Porto, G., and De Sousa, M. (2007) Iron overload and immunity. *World J. Gastroenterol. 13*, 4707–4715.
48. Macedo, M. F., De Sousa, M., Ned, R. M., Mascarenhas, C., Andrews, N. C., and Correia-Neves, M. (2004) Transferrin is required for early T-cell differentiation. *Immunology 112*, 543–549.
49. Pace, C. N., Vajdos, F., Fee, L., Grimsley, G., and Gray, T. (1995) How to measure and predict the molar absorption coefficient of a protein. *Protein Sci. 4*, 2411–2423.
50. Edelhoch, H. (1967) Spectroscopic Determination of Tryptophan and Tyrosine in Proteins. *Biochemistry 6*, 1948–1954.

BI801133D